Letter | Editors' Suggestion

# Quantum gas microscopy of fermionic triangular-lattice Mott insulators

Jirayu Mongkolkiattichai, Liyu Liu, Davis Garwood, Jin Yang,* and Peter Schauss†
*Department of Physics, University of Virginia, Charlottesville, Virginia 22904, USA*

(Received 17 February 2023; revised 4 July 2023; accepted 13 November 2023; published 13 December 2023)

We investigate fermionic Mott insulators in a geometrically frustrated triangular lattice, a paradigm model system for studying spin liquids and spontaneous time-reversal symmetry breaking. Our study demonstrates the preparation of triangular Mott insulators and reveals antiferromagnetic spin-spin correlations among all nearest neighbors. We employ a real-space triangular-geometry quantum gas microscope to measure density and spin observables. Comparing experimental results with calculations based on numerical linked cluster expansions and quantum Monte Carlo techniques, we demonstrate thermometry in the frustrated system. Our experimental platform introduces an alternative approach to frustrated lattices which paves the way for future investigations of exotic quantum magnetism which may lead to a direct detection of quantum spin liquids in Hubbard systems.

DOI: 10.1103/PhysRevA.108.L061301

Electronic systems typically establish long-range order at zero temperature. Surprisingly, there are systems that do not have this fundamental property. For example, quantum spin liquids [1,2] form in the presence of conflicting energetic constraints that prevent long-range ordering. Interestingly, the absence of ordering opens the door to a variety of exotic phenomena. Quantum spin liquids can show fractional quasiparticle statistics analogous to those underlying the quantum Hall effect [3].

Time-reversal symmetry breaking has been predicted in numerical studies on frustrated systems and kinetic constraints caused by the frustration lead to complex time-evolution [4–6]. While frustrated systems with small number of particles can be accurately simulated with tremendous computational resources, predictions for the low-temperature phases in the thermodynamic limit are scarce and often debated [7–9]. Existing condensed-matter realizations are complicated materials [4], making well-controlled model systems a valuable alternative for gaining insight into the physics of frustration.

Ultracold atoms provide a unique way to explore quantum many-body physics through quantum simulation based on first principles. Prominent examples of quantum simulation with ultracold atoms include the realization of Hubbard models [10] and the observation of many-body localization [11]. While there is widespread evidence for insulating phases without magnetic ordering in frustrated Hubbard models, their existence and properties are still controversial on many lattice geometries, including the triangular lattice which has been proposed as paradigm model for geometric frustration [2]. Ultracold atoms in optical lattices implement Hubbard models [10,12,13], where neighboring sites are coupled by hopping, and atoms on the same lattice site interact. Atomic Fermi-Hubbard systems were first realized with ultracold atoms in square lattices [14,15]. With the realization of quantum gas microscopes for fermions, it became possible to image fermionic atoms on the single-atom level [16–20]. Later, two-dimensional (2d) fermionic Mott insulators (MIs) were detected with quantum gas microscopes using $^6$Li [21] and $^{40}$K [22]. In particular, the characteristic antiferromagnetic correlations in the repulsive Hubbard model have been investigated in detail [23–29]. Frustration has been studied with various ultracold atomic systems, starting with Bose-Einstein condensates in frustrated lattices [30,31] and recently by the realization of frustrated spin systems with Rydberg atoms in optical tweezers [32,33]. Here, we expand quantum simulation of frustrated systems to fermions in a Hubbard model on a triangular-lattice structure and report on the site-resolved imaging of fermionic atomic Mott insulators in a triangular lattice. Although the triangular geometry suppresses antiferromagnetic ordering, short-range correlations persist over a wide range of parameters, and we measure these correlations and perform thermometry by comparison with numerical calculations, realizing for the first time a detailed comparison between theory and experiment of the equilibrium properties of the triangular Hubbard model in an optical lattice. Our work establishes a novel platform for the study of frustrated Hubbard physics.

The Hamiltonian of the fermionic system in a two-dimensional lattice at half filling is $\mathcal{H} = -t \sum_{\langle \mathbf{r}\mathbf{r}' \rangle,\sigma} (c^\dagger_{\mathbf{r},\sigma} c_{\mathbf{r}',\sigma} + c^\dagger_{\mathbf{r}',\sigma} c_{\mathbf{r},\sigma}) + U \sum_{\mathbf{r}} n_{\mathbf{r},\uparrow} n_{\mathbf{r},\downarrow} - \mu(\mathbf{r}) \sum_{\mathbf{r}} (n_{\mathbf{r},\uparrow} + n_{\mathbf{r},\downarrow})$, where $t$ is the tunneling strength between nearest-neighbor lattice sites, $U$ is the on-site interaction, $c_{\mathbf{r},\sigma}$ ($c^\dagger_{\mathbf{r}',\sigma}$) is the annihilation (creation) operator for a fermion with spin $\sigma$ on site $\mathbf{r}$, $n_{\mathbf{r},\sigma} = c^\dagger_{\mathbf{r},\sigma} c_{\mathbf{r},\sigma}$ is the number operator, and $\mu(\mathbf{r})$ is the chemical potential. This model describes the transition from a metal to a fermionic Mott Insulator. The insulating behavior originates from the electron-electron correlations and cannot be explained in a noninteracting electron picture. At temperatures below $U/k_B$, double occupation of sites is suppressed. Single occupation is

*Present address: Department of Physics, Research Laboratory of Electronics, MIT-Harvard Center for Ultracold Atoms, Massachusetts Institute of Technology, Cambridge, Massachusetts 02139, USA; dypole_jin@mit.edu
†ps@virginia.edu

 

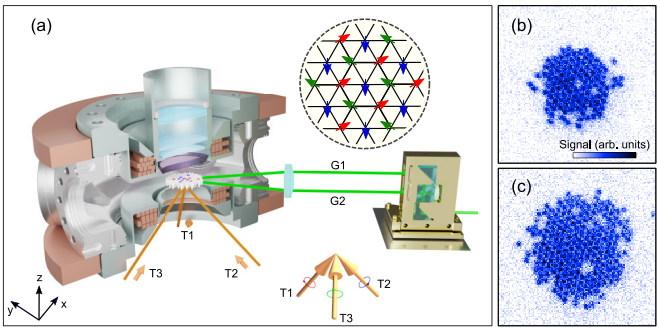


FIG. 1. Triangular-lattice quantum gas microscope. (a) A triangular optical lattice is realized by interfering three circularly polarized laser beams ($T1$, $T2$, and $T3$) using 1064 nm light in the center of a vacuum chamber. The confinement of the atoms into two dimensions is achieved by a 1d accordion lattice in vertical direction, formed by the 532 nm laser beams $G1$ and $G2$. A combination of a beam splitter and mirrors allows us to vary the distance between $G1$ and $G2$ via the height of the input beam, therefore forming a lattice with a variable spacing between 3 and 8 μm. A high-resolution objective enables single-site resolved imaging of the atoms in the triangular lattice. The inset demonstrates 120° order which is the classical analog of the spin ordering expected at large interactions. (b), (c) Triangular-lattice Mott insulators at $U/t = 10(1)$ with 109 atoms (top right) and $U/t = 26(3)$ with 203 atoms (bottom right). The field of view is 32 μm × 32 μm.

energetically preferred at $\mu \sim U/2$ and the density variance approaches zero, leading to a MI. When the chemical potential is larger than the energy gap, doublons (two atoms on a site) are formed. They first appear at the center of the trap, forming a band insulating core, because of the lower harmonic potential. More than two atoms per site in the lowest band are forbidden by the Pauli exclusion principle, and higher band population is strongly suppressed energetically at such low temperatures. Short-range antiferromagnetic ordering can be observed in MIs when the temperature is comparable to the exchange energy $J = 4t^2/U$ [34]. In this study, we acquired experimental data in this temperature regime, demonstrated consistency of numerical calculations and measurements characterizing the equation of state of the triangular Hubbard model, and observed antiferromagnetic correlations on the triangular lattice.

We started the experiment by preparing a spin-balanced Fermi gas in a single layer of a one-dimensional (1d) accordion lattice [Fig. 1(a)] with a variable spacing. The gas is a mixture of the two lowest hyperfine ground states $|\uparrow\rangle = |F = 1/2, m_F = 1/2\rangle$ and $|\downarrow\rangle = |F = 1/2, m_F = -1/2\rangle$ of $^6$Li, where $F$ and $m_F$ are the hyperfine quantum numbers [35]. Next, the atoms are adiabatically loaded into the triangular lattice of depth $9.7(6)E_R$. Here, $E_R = \hbar^2\pi^2/(2ma_{\text{latt}}^2) = h \times 8.2\,\text{kHz}$ is the recoil energy where $h$ is Planck's constant, $m$ is the atomic mass, and $a_{\text{latt}} = 1003$ nm. The tunneling parameter is $t = h \times 436(40)\,\text{Hz}$ [35]. The atom number and density in the lattice is adjustable by varying evaporation parameters. Once the atoms are in the lattice, we tune the scattering length to $525(4)a_0$, where $a_0$ is the Bohr radius, thereby adjusting the interaction to $U/t = 10(1)$. To detect the singles density ($n^s = n - n_\uparrow n_\downarrow$), the atom motion is frozen by linearly increasing the lattice depth up to $100E_R$. For imaging, we turn off all magnetic fields and switch to maximum lattice depth $\approx 10^4 E_R$. Images of MIs for different interaction strengths are shown in Figs. 1(b) and 1(c).

By varying the atom number loaded into the lattice, we observe MI and band insulators (BIs) at $U/t = 10(1)$ (Fig. 2). The MI region [Fig. 2(b)] has nearly unit filling and atom number fluctuations are suppressed. When the chemical potential $\mu$ exceeds the value of $U/2$ (approximately half filling), doubly occupied sites are formed, therefore a BI region in the center of the trap forms, as shown in Figs. 2(c) and 2(d). Doubly occupied sites are detected as empty sites due to light-assisted collisions at the imaging stage [21].

To access the singles density profile, we perform a deconvolution to determine the site occupation numbers and obtain singles density ($n^s$) and variance ($\sigma^2_{n^s}$) via azimuthal averaging (bottom panel of Fig. 2). We fit the experimental density profile using determinantal quantum Monte Carlo (DQMC) and numerical linked cluster expansion (NLCE) calculations [35]. The temperature and chemical potential of the atoms in the trap are free parameters in the nonlinear least-squares fitting. We find good agreement with a global fit relying on a local density approximation using $\mu(\mathbf{r}) = \mu_0 - \frac{1}{2}m\omega^2 r^2$ [35]. The results of the fitting can be found in Fig. 2. We observe a small deviation at the center of the trap, which we attribute to the lower statistics and the uncertainty in the determination of the exact center of the system for azimuthal averaging. We observe an increased temperature for larger atom numbers as a result of reduced evaporative cooling. Lifetime measurements in the lattice show no significant density-dependent heating.

Spin-spin correlations have proven to be essential observables for the understanding of the Hubbard model on square lattices [26–29]. The spin-spin correlator is defined as $C^z_{\mathbf{a}}(\mathbf{r}) = 4(\langle S^z_{\mathbf{r}} S^z_{\mathbf{r}+\mathbf{a}}\rangle - \langle S^z_{\mathbf{r}}\rangle\langle S^z_{\mathbf{r}+\mathbf{a}}\rangle)$, where the spin operator is $S^z_{\mathbf{r}} = (n_{\mathbf{r},\uparrow} - n_{\mathbf{r},\downarrow})/2$. Here, the parameter $\mathbf{a}$ denotes the shift in the lattice site number between the two correlated positions, and $\mathbf{r}$ is the current lattice site. We access the observable $C^z_{\mathbf{a}}(\mathbf{r})$ via a linear combination of different correlators that can be measured directly in the experiment [35].

The fate of antiferromagnetic correlations on frustrated lattices is not obvious because the ordering is not compatible with the lattice structure. Despite the geometric frustration, we find significant antiferromagnetic correlations at nearest-neighbor sites although our temperatures are above the exchange energy scale $J = 4t^2/U \approx 0.4t$. The reduced antiferromagnetic correlation compared with the maximal correlation of $-1$ can be interpreted as incomplete antialignment of the spins. At large interactions, the Hubbard model maps to the Heisenberg model, and 120° order is expected [Fig. 1(a)]. Negative nearest-neighbor correlations of $C^z_{\mathbf{b1}} = -0.078(22)$, $C^z_{\mathbf{b2}} = -0.053(23)$, and $C^z_{\mathbf{b1}-\mathbf{b2}} = -0.071(28)$ are observed for three directions ($\mathbf{b1}$, $\mathbf{b2}$, and $\mathbf{b1} - \mathbf{b2}$) as depicted in Fig. 3(a) [35]. We compare the experimental data with a correlation map calculated by DQMC at $U/t = 10$ and $k_BT/t = 0.8$ [Fig. 3(b)]. The calculated nearest-neighbor spin-spin correlations agree with the experimental data within error bars. The observed negative correlations among all nearest neighbors is consistent with 120° order. Next-nearest-neighbor spin-spin correlations in the experimental data are consistent with zero within the

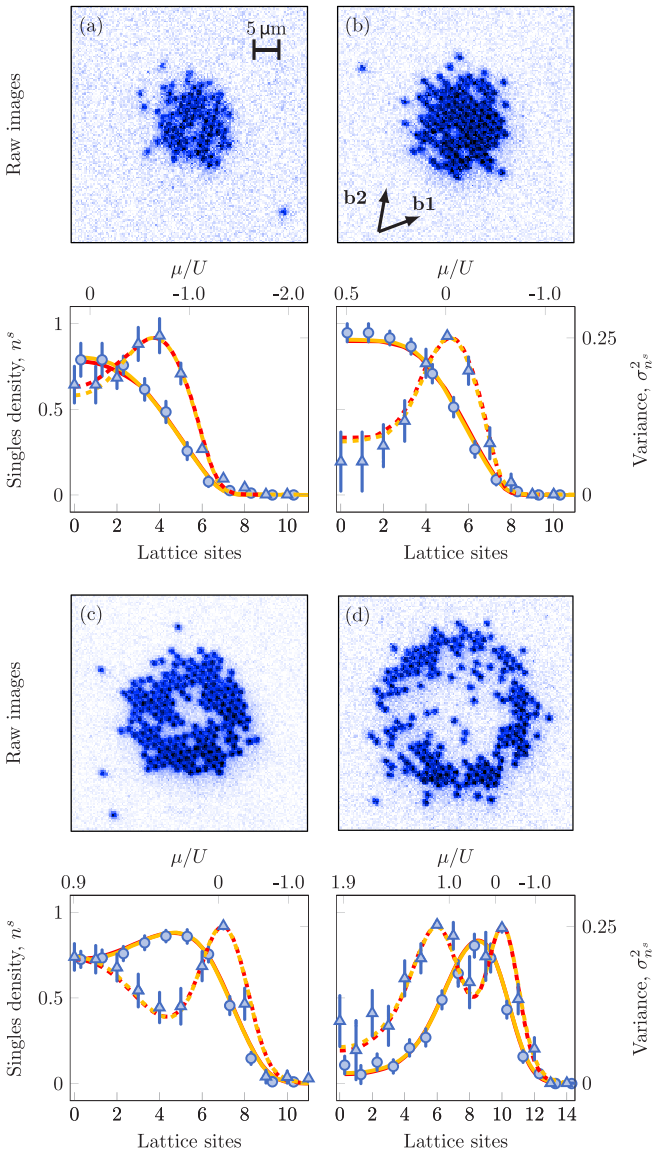


FIG. 2. Triangular-lattice Mott insulators. (a)–(d) (top) Site-resolved fluorescence images of fermionic Mott insulators with increasing atom number integrated from fit, 77, 119, 175, and 183 at interaction $U/t = 10(1)$. (a)–(d) (bottom) Comparison of azimuthally averaged singles density (dots) and variance (triangles) with theory calculations, QMC (red) and NLCE (orange). The data points of the variance are horizontally offset by 0.3 lattice sites for clarity. Both singles density $n^s$ and variance $\sigma^2_{n^s}$ are fit with QMC and NLCE theory using the local density approximation [35]. The detected variance is the square of the standard deviation of the sample within a radial bin. The fits yield temperatures $k_BT/t = 0.9(2)$, 0.9(1), 1.5(1), and 2.4(1) with chemical potentials $\mu_0/U = 0.24(10)$, 0.5(4), 0.91(3), and 1.94(1), respectively, at the trap center for increasing atom number in both QMC and NLCE calculations. Error bars on $n^s$ are the standard error of the mean and error bars on $\sigma^2_{n^s}$ are determined by error propagation from $\sigma^2_{n^s} = n^s - (n^s)^2$.

typical uncertainty of 0.02, which we believe is limited by the currently realized temperatures in our experiment. Compared with the square lattice, where nearest-neighbor spin-spin correlation alternate in sign, the spin-spin correlations in the triangular lattice are smaller in magnitude and negative for all

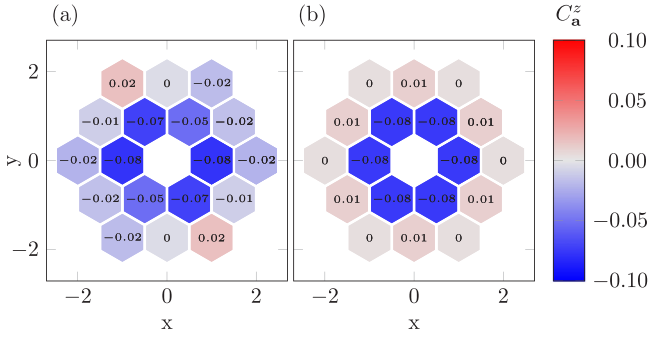


FIG. 3. Spin-spin correlations. (a) Experimental correlations for $U/t = 10\,(1)$. The $C^z_{\mathbf{b1}}$, $C^z_{\mathbf{b2}}$, and $C^z_{\mathbf{b1-b2}}$ are observed as anticorrelated along (1,0), $(1/2, \sqrt{3}/2)$, and $(1/2, -\sqrt{3}/2)$. These values are the same within error bars suggesting tunneling isotropy of our triangular lattice. The correlations are extracted with postselection from 400 experimental pictures [35]. Typical values of experimental error bars are ≈0.02 and evaluated by bootstrap. (b) Spin-spin correlations between nearest and next-nearest lattice sites calculated by DQMC at a temperature of $k_BT/t = 0.8$ near half filling and $C^z_0$ is omitted for clarity. DQMC theory shows good agreement with experiment. The measured next-nearest-neighbor spin-spin correlations are consistent with zero within error bars.

nearest neighbors in the same parameter regimes, which we attribute to the geometrically frustrated triangular structure.

To extract the temperature, we perform azimuthal averaging of nearest-neighbor correlations as a function of the distance from the trap center along the equipotential of the lattice confinement [35] and fit to DQMC and NLCE calculations using temperature and chemical potential at the trap center as free parameters [Fig. 4(a)]. We also average the correlations along the three lattice axes because they are equal within error bars. We show the result as a band in Fig. 4(b) and obtain a temperature of $k_BT/t \approx 0.8$ by comparing correlations between experiment and theory calculations at half filling. The measured temperature is consistent with the radial singles density fit in Fig. 2 with half filling at the center of the system.

This temperature is clearly below the interaction energy $U/t = 10(1)$, and lower than the tunneling energy scale and therefore quantum effects in the motion and interaction of the atoms can be observed. From comparisons to square lattice Mott insulators in our apparatus, we attribute the elevated temperature partially to the more complex lattice beam geometry which relies on the interference of three laser beams. Obtaining high contrast in three-beam interference is more sensitive to polarization purity and air-movement-induced beam pointing than for two-beam interference. The resulting time-dependence of the lattice potential leads to heating. Heating and thermalization in triangular lattices, as well as the loading dynamics into the lattice, merit further theoretical and experimental study in the future.

In Fig. 4(c), we demonstrate our ability to tune interactions. The strongest nearest-neighbor spin-spin correlations in the triangular lattice are found for $U/t \approx 10$, whereas the strongest correlations in the square lattice occur near $U/t \approx 8$ Ref. [28]. We observe atom loss when increasing the scattering length beyond a value of $\approx 650 a_0$. Therefore, we change

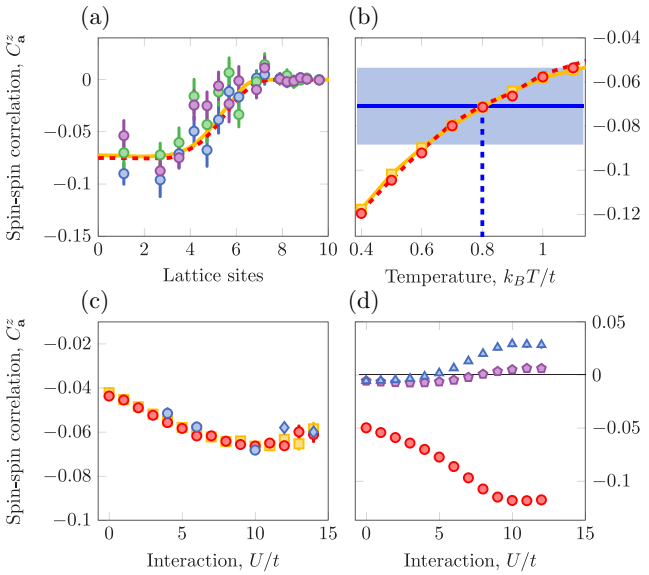


FIG. 4. Thermometry and interaction dependence of spin-spin correlations. (a) Spatial variation of nearest-neighbor correlations. Blue, violet and green dots are measured correlations along $\mathbf{a} = \mathbf{b1}$, $\mathbf{b2}$, and $\mathbf{b1} - \mathbf{b2}$, respectively. We perform an azimuthal average along the equipotential of the lattice confinement. The experimental data is fit to DQMC (red dashed line) and NLCE (orange solid line) and we extract a temperature $k_BT/t = 0.80(10)$. Error bars are the standard error of the mean. (b) Nearest-neighbor spin-spin correlation as a function of temperature. The experimental correlations at the center of the trap are visualized by the light-blue shaded band with average indicated by the blue line compared with calculations from DQMC (red dots) and NLCE (orange squares) at half filling. Orange solid and red dashed lines are a guide to the eye. The width of the blue band indicates the error of nearest-neighbor spin-spin correlation evaluated by the error propagation of nearest-neighbor spin-spin correlations established in Fig. 3(b). We find $k_BT/t = 0.80(25)$ (blue dashed line). (c) Interaction dependence of nearest-neighbor spin-spin correlations. Measured correlations (blue dots) are compared with DQMC (red dots) and NLCE (orange square) theory for temperature $k_BT/t \approx 0.9$ at half filling. Blue diamonds are measured using lattice depth of $12.0(7)E_R$ to avoid losses at large values of $U$ [35]. Error bars are the standard error of the mean evaluated by bootstrap [35]. (d) DQMC calculation of spin-spin correlations at $k_BT/t = 0.4$ at half filling for shifts (1,0), (1.5,0.9), and (2,0) (red dots, blue triangles, and violet pentagons, respectively). The next-nearest-neighbor spin-spin correlations show a sign change versus $U/t$.

the lattice depth to reach larger $U/t$ [35]. We find good agreement with theory and note that the experimental temperature $k_BT/t \approx 0.9$ is almost independent of $U/t$.

Next-nearest-neighbor spin-spin correlations are challenging to measure as can be seen in Fig. 4(d). DQMC calculations show a suppression of spin-spin correlations for next-nearest neighbors by a factor of eight compared with that for nearest neighbors at a temperature $k_BT/t = 0.4$ and half filling. As interactions are increased, the next-nearest-neighbor spin-spin correlations are expected to cross over from negative in a possible spin-liquid regime to positive in the 120° ordered phase in contrast to the situation in 2d square lattices at half filling [26–28]. Experimental temperatures around $k_BT/t = 0.4$ or lower would therefore allow for the detection of next-nearest neighbor correlations and may make it possible to distinguish predictions for 120° order and spin liquid correlations.

In conclusion, we prepared fermionic Mott insulators on a triangular optical lattice and performed single-site resolved imaging to detect spin-spin correlations which allow us to infer the temperature of our systems. The radial density profiles of the observed Hubbard systems are in agreement with DQMC and NLCE calculations. Reducing the temperatures in our system is an outstanding challenge. Possible ways to significantly reduce the temperature are a redesign of the trapping configuration during the final evaporation, the implementation of entropy redistribution techniques [36] or the addition of $^7$Li to the system for sympathetic cooling [37]. Future experiments will access spin-density correlations to study kinetic magnetism [27,38,39], enabling the study of polarons with special properties caused by the frustrated nature of the triangular lattice [40–42]. Binding energies are expected to scale with the tunneling $t$ and may be detectable at higher temperatures compared with square lattices [41]. Systems with increased binding energy are interesting because they may provide a path towards realizing repulsive pairing at higher temperatures and, therefore, higher-temperature superconductivity. Additional future directions where our experimental platform can challenge state-of-the-art numerical calculations include the study of transport properties [43] and the experimental search for chiral ordering predicted for triangular Hubbard systems [3,9].

*Note added.* Recently, related work on triangular fermionic Mott insulators by Xu *et al.* appeared [44].

*Acknowledgments.* We thank Gia-Wei Chern, Bob Jones, and Cass Sackett for careful reading of the paper. We thank Cass Sackett for sharing equipment. We acknowledge support by the NSF (CAREER Award No. 2047275), ONR (DURIP Award No. N00014-22-1-2681), the Thomas F. and Kate Miller Jeffress Memorial Trust and the Jefferson Trust. D.G. was supported by a Ingrassia Scholarship. J.M. acknowledges support by The Beitchman Award for Innovative Graduate Student Research in Physics in honor of Robert V. Coleman and Bascom S. Deaver, Jr.

J.M. and L.L. contributed equally to this work.

[1] G. H. Wannier, Antiferromagnetism. The triangular Ising net, Phys. Rev. **79**, 357 (1950).

[2] P. W. Anderson, The resonating valence bond state in $La_2CuO_4$ and superconductivity, Science **235**, 1196 (1987).

[3] X. G. Wen, F. Wilczek, and A. Zee, Chiral spin states and superconductivity, Phys. Rev. B **39**, 11413 (1989).

[4] L. Balents, Spin liquids in frustrated magnets, Nature (London) **464**, 199 (2010).

[5] C. D. Batista, S.-Z. Lin, S. Hayami, and Y. Kamiya, Frustration and chiral orderings in correlated electron systems, Rep. Prog. Phys. **79**, 084504 (2016).

[6] Y. Zhou, K. Kanoda, and T.-K. Ng, Quantum spin liquid states, Rev. Mod. Phys. **89**, 025003 (2017).

[7] T. Yoshioka, A. Koga, and N. Kawakami, Quantum phase transitions in the Hubbard model on a triangular lattice, Phys. Rev. Lett. **103**, 036401 (2009).

[8] T. Shirakawa, T. Tohyama, J. Kokalj, S. Sota, and S. Yunoki, Ground-state phase diagram of the triangular lattice Hubbard model by density matrix renormalization group method, Phys. Rev. B **96**, 205130 (2017).

[9] A. Szasz, J. Motruk, M. P. Zaletel, and J. E. Moore, Chiral spin liquid phase of the triangular lattice Hubbard model: A density matrix renormalization group study, Phys. Rev. X **10**, 021042 (2020).

[10] I. Bloch, J. Dalibard, and W. Zwerger, Many-body physics with ultracold gases, Rev. Mod. Phys. **80**, 885 (2008).

[11] C. Gross and I. Bloch, Quantum simulations with ultracold atoms in optical lattices, Science **357**, 995 (2017).

[12] M. Lewenstein, A. Sanpera, V. Ahufinger, B. Damski, A. Sen(De), and U. Sen, Ultracold atomic gases in optical lattices: Mimicking condensed matter physics and beyond, Adv. Phys. **56**, 243 (2007).

[13] T. Esslinger, Fermi-Hubbard physics with atoms in an optical lattice, Annu. Rev. Condens. Matter Phys. **1**, 129 (2010).

[14] R. Jördens, N. Strohmaier, K. Günter, H. Moritz, and T. Esslinger, A Mott insulator of fermionic atoms in an optical lattice, Nature (London) **455**, 204 (2008).

[15] U. Schneider, L. Hackermüller, S. Will, T. Best, I. Bloch, T. A. Costi, R. W. Helmes, D. Rasch, and A. Rosch, Metallic and insulating phases of repulsively interacting fermions in a 3D optical lattice, Science **322**, 1520 (2008).

[16] L. W. Cheuk, M. A. Nichols, M. Okan, T. Gersdorf, V. V. Ramasesh, W. S. Bakr, T. Lompe, and M. W. Zwierlein, Quantum-gas microscope for fermionic atoms, Phys. Rev. Lett. **114**, 193001 (2015).

[17] M. F. Parsons, F. Huber, A. Mazurenko, C. S. Chiu, W. Setiawan, K. Wooley-Brown, S. Blatt, and M. Greiner, Site-resolved imaging of fermionic $^{6}$Li in an optical lattice, Phys. Rev. Lett. **114**, 213002 (2015).

[18] E. Haller, J. Hudson, A. Kelly, D. A. Cotta, B. Peaudecerf, G. D. Bruce, and S. Kuhr, Single-atom imaging of fermions in a quantum-gas microscope, Nat. Phys. **11**, 738 (2015).

[19] G. J. A. Edge, R. Anderson, D. Jervis, D. C. McKay, R. Day, S. Trotzky, and J. H. Thywissen, Imaging and addressing of individual fermionic atoms in an optical lattice, Phys. Rev. A **92**, 063406 (2015).

[20] A. Omran, M. Boll, T. A. Hilker, K. Kleinlein, G. Salomon, I. Bloch, and C. Gross, Microscopic observation of Pauli blocking in degenerate fermionic lattice gases, Phys. Rev. Lett. **115**, 263001 (2015).

[21] D. Greif, M. F. Parsons, A. Mazurenko, C. S. Chiu, S. Blatt, F. Huber, G. Ji, and M. Greiner, Site-resolved imaging of a fermionic Mott insulator, Science **351**, 953 (2016).

[22] L. W. Cheuk, M. A. Nichols, K. R. Lawrence, M. Okan, H. Zhang, and M. W. Zwierlein, Observation of 2D fermionic Mott insulators of $^{40}$K with single-site resolution, Phys. Rev. Lett. **116**, 235301 (2016).

[23] D. Greif, T. Uehlinger, G. Jotzu, L. Tarruell, and T. Esslinger, Short-range quantum magnetism of ultracold fermions in an optical lattice, Science **340**, 1307 (2013).

[24] R. A. Hart, P. M. Duarte, T.-L. Yang, X. Liu, T. Paiva, E. Khatami, R. T. Scalettar, N. Trivedi, D. A. Huse, and R. G. Hulet, Observation of antiferromagnetic correlations in the Hubbard model with ultracold atoms, Nature (London) **519**, 211 (2015).

[25] J. H. Drewes, L. A. Miller, E. Cocchi, C. F. Chan, N. Wurz, M. Gall, D. Pertot, F. Brennecke, and M. Köhl, Antiferromagnetic correlations in two-dimensional fermionic Mott-insulating and metallic phases, Phys. Rev. Lett. **118**, 170401 (2017).

[26] M. F. Parsons, A. Mazurenko, C. S. Chiu, G. Ji, D. Greif, and M. Greiner, Site-resolved measurement of the spin-correlation function in the Fermi-Hubbard model, Science **353**, 1253 (2016).

[27] M. Boll, T. A. Hilker, G. Salomon, A. Omran, J. Nespolo, L. Pollet, I. Bloch, and C. Gross, Spin- and density-resolved microscopy of antiferromagnetic correlations in Fermi-Hubbard chains, Science **353**, 1257 (2016).

[28] L. W. Cheuk, M. A. Nichols, K. R. Lawrence, M. Okan, H. Zhang, E. Khatami, N. Trivedi, T. Paiva, M. Rigol, and M. W. Zwierlein, Observation of spatial charge and spin correlations in the 2D Fermi-Hubbard model, Science **353**, 1260 (2016).

[29] P. T. Brown, D. Mitra, E. Guardado-Sanchez, P. Schauß, S. S. Kondov, E. Khatami, T. Paiva, N. Trivedi, D. A. Huse, and W. S. Bakr, Spin-imbalance in a 2D Fermi-Hubbard system, Science **357**, 1385 (2017).

[30] J. Struck, C. Ölschläger, R. L. Targat, P. Soltan-Panahi, A. Eckardt, M. Lewenstein, P. Windpassinger, and K. Sengstock, Quantum simulation of frustrated classical magnetism in triangular optical lattices, Science **333**, 996 (2011).

[31] J. Struck, M. Weinberg, C. Ölschläger, P. Windpassinger, J. Simonet, K. Sengstock, R. Höppner, P. Hauke, A. Eckardt, M. Lewenstein, and L. Mathey, Engineering Ising-$XY$ spin-models in a triangular lattice using tunable artificial gauge fields, Nat. Phys. **9**, 738 (2013).

[32] P. Scholl, M. Schuler, H. J. Williams, A. A. Eberharter, D. Barredo, K.-N. Schymik, V. Lienhard, L.-P. Henry, T. C. Lang, T. Lahaye, A. M. Läuchli, and A. Browaeys, Quantum simulation of 2D antiferromagnets with hundreds of Rydberg atoms, Nature (London) **595**, 233 (2021).

[33] G. Semeghini, H. Levine, A. Keesling, S. Ebadi, T. T. Wang, D. Bluvstein, R. Verresen, H. Pichler, M. Kalinowski, R. Samajdar, A. Omran, S. Sachdev, A. Vishwanath, M. Greiner, V. Vuletić, and M. D. Lukin, Probing topological spin liquids on a programmable quantum simulator, Science **374**, 1242 (2021).

[34] A. Auerbach, *Interacting Electrons and Quantum Magnetism* (Springer, New York, 1990).

[35] See Supplemental Material at http://link.aps.org/supplemental/10.1103/PhysRevA.108.L061301 for details on experiment, data analysis, Hubbard parameter calibration, and on the numerical calculations.

[36] A. Mazurenko, C. S. Chiu, G. Ji, M. F. Parsons, M. Kanász-Nagy, R. Schmidt, F. Grusdt, E. Demler, D. Greif, and M. Greiner, A cold-atom Fermi–Hubbard antiferromagnet, Nature (London) **545**, 462 (2017).

[37] I. Ferrier-Barbut, M. Delehaye, S. Laurent, A. T. Grier, M. Pierce, B. S. Rem, F. Chevy, and C. Salomon, A mixture of Bose and Fermi superfluids, Science **345**, 1035 (2014).

[38] J. Koepsell, S. Hirthe, D. Bourgund, P. Sompet, J. Vijayan, G. Salomon, C. Gross, and I. Bloch, Robust bilayer charge pumping for spin- and density-resolved quantum gas microscopy, Phys. Rev. Lett. **125**, 010403 (2020).

[39] I. Morera, M. Kanász-Nagy, T. Smolenski, L. Ciorciaro, A. Imamoğlu, and E. Demler, High-temperature kinetic magnetism in triangular lattices, Phys. Rev. Res. **5**, L022048 (2023).

[40] M. Vojta, Spin polarons in triangular antiferromagnets, Phys. Rev. B **59**, 6027 (1999).

[41] S.-S. Zhang, W. Zhu, and C. D. Batista, Pairing from strong repulsion in triangular lattice Hubbard model, Phys. Rev. B **97**, 140507(R) (2018).

[42] J. van de Kraats, K. K. Nielsen, and G. M. Bruun, Holes and magnetic polarons in a triangular lattice antiferromagnet, Phys. Rev. B **106**, 235143 (2022).

[43] A. Vranić, J. Vučičević, J. Kokalj, J. Skolimowski, R. Žitko, J. Mravlje, and D. Tanasković, Charge transport in the Hubbard model at high temperatures: Triangular versus square lattice, Phys. Rev. B **102**, 115142 (2020).

[44] M. Xu, L. H. Kendrick, A. Kale, Y. Gang, G. Ji, R. T. Scalettar, M. Lebrat, and M. Greiner, Frustration- and doping-induced magnetism in a Fermi–Hubbard simulator, Nature (London) **620**, 971 (2023).